

Towards Solving Industry-Grade Surrogate Modeling Problems using Physics Informed Machine Learning

Saakaar Bhatnagar^{a†}

shatnagar@altair.com

Andrew Comerford^a

acomerford@altair.com

Araz Banaeizadeh^a

araz@altair.com

^aAltair Engineering Inc., 100 Mathilda Place, Sunnyvale, CA, USA

Keywords: Surrogate Modeling; Physics-Based Machine Learning; Physics Informed Neural Networks; Design of Experiments; Design Optimization; Electronics Thermal Design

Abstract

Deep learning combined with physics-based modeling represents an attractive and efficient approach for producing accurate and robust surrogate modeling. In this paper, a new framework that utilizes Physics Informed Neural Networks (PINN) to solve PDE-based problems for the creation of surrogate models for steady-state flow-thermal engineering design applications is introduced. The surrogate models developed through this framework are demonstrated on several use cases from electronics cooling to biomechanics. Additionally, it is demonstrated how these trained surrogate models can be combined with design optimization methods to improve the efficiency and reduced the cost of the design process. The former is shown through several realistic 3D examples and the latter via a detailed cost-benefit trade off. Overall, the findings of this paper demonstrate that hybrid data-PINN surrogate models combined with optimization algorithms can solve realistic design optimization and have potential in a wide variety of application areas.

1 Introduction

Over the last few years, there has been significant growth in the popularity of machine learning algorithms to solve partial differential equations (PDE) or assist PDE solvers, such as a computational fluid dynamics(CFD) solver [7, 10]. The attraction of ML algorithms in these scenarios is the ability to find solutions in domains that are challenges in conventional CFD, such as large design space explorations [37], turbulence model closure [73] or solving incomplete/ill-posed problems [9].

A particular application where CFD solvers struggle, due to the computational cost, is iterative design optimization. This is the process of continually updating a design (e.g. an electronics assembly layout) and computing the solution (e.g. flow or thermal fields) to optimize the performance (e.g. constrain the temperatures or reduce the pressure drop). The challenge for CFD is the input-output relationship is one-to-one. Therefore, any changes to the input vector (e.g. geometric variations) need to be re-simulated, leading to high costs when iterating on different design scenarios [31]. Overall high-fidelity iterative design requires a prohibitive level of resources, both computationally and monetarily and often leads to a sub-optimal outcome.

To enhance the iterative design process and speed up CFD simulations surrogate models are usually utilized. Surrogate modeling represents an essential simulation technology for many computationally expensive applications. In literature, there has been a significant amount of research on the construction of surrogate or reduced order models using simulation data [32], [20]; these methods include Proper Orthogonal Decomposition(POD) [32], Gappy POD [42], Manifold Learning [40]. These approaches serve as good surrogates that give near real-time predictions for input parameters within a certain range. However, these methods have remained largely academic in their application due to limitations, such as training data requirements and only working in simple scenarios. Recently, increased attention has been given to statistical methods like Gaussian processes and neural networks

[†]Corresponding Author

that incorporate Machine Learning (ML) to create the same surrogates. Bhatnagar et al. [4] used a CNN architecture to predict aerodynamic flow fields over airfoils, and created a surrogate model that generalized between flow conditions and airfoil geometries. Guo et al. [22] also used a Convolutional Neural Network (CNN) architecture to predict steady flows over automotive vehicles. Lee and You [34] used Generative Adversarial Networks(GANs) coupled with physical laws to predict unsteady flow around a cylinder, demonstrating the benefits of using embedded physics. Raissi and Karniadakis [50] uses Gaussian processes to model and identify several complex PDEs.

Machine learning, and more specifically Artificial Neural Networks (ANNs), have seen success in areas such as computer vision, natural language processing and healthcare [14, 51, 63]. Much of this success can be attributed to the development of new model architectures, programming frameworks (e.g. Tensorflow and PyTorch), and most importantly large training datasets. The ability of ANNs to capture complex nonlinear relationships between inputs and outputs have also made them very well-suited for regression problems. For design engineering applications, the ANN-based surrogate model must be consistent with the underlying physics; however, to achieve this, a number of hurdles must be overcome:

1. **Data is Expensive:** Unlike many other commercial applications, solution data to create surrogate models is generally expensive to obtain. Typically, the data is obtained through repetitive simulation. Since ANNs work best with large amounts of data to train them, this makes the cost of conventional data-driven modeling via ANNs expensive.
2. **Spectral Bias:** It is a well-documented feature of ANNs [11, 48, 62] that they possess a bias towards learning the lower frequencies of a signal they are being trained on first. This leads to a more challenging training process for ANNs for engineering problems, where it is important to capture these high-frequency components of the solution in an economical manner.
3. **Multiphysics and Multiscale problems:** Many engineering applications, especially in the flow-thermal realm, are multiscale in nature with complex flow physics that need to be captured by surrogate models. This is not straightforward and requires special treatment to ensure the generalizability of the model [13, 28], as well as the correctness of the solution across any interfaces.
4. **Unphysical Results:** Purely data-driven models may not end up learning the underlying physics from the data. This leads to unphysical results when trying to generalize to unseen test cases with these models.

In order to build scalable, robust surrogate models using ANNs for general engineering design problems, the above challenges need to be addressed. The ideal surrogate model must satisfy the following criteria: 1) limited input data; 2) generalizable; 3) easy and economical to create; and 4) parallelizable.

In this paper, the Altair framework for flow-thermal surrogate model creation and automatic design optimization is presented. The aforementioned difficulties are individually addressed with a number of different proposed solutions while addressing the lack of research applying physics-informed ML to problems closer to the complexity of industrial design problems. The effectiveness of adding very sparse solution data in the domain to aid Physics Informed Neural Network convergence in 3D is demonstrated for a complex geometry at a high Reynolds Number. Additionally, flow through a stenosis is solved at a Reynolds Number of 150 in 3 dimensions, done with realistic physical parameters in a purely physics-informed manner. Finally, a novel method of coupling physics-informed ANN surrogates with traditional design optimization algorithms (e.g. Particle Swarm Optimization [29]) is presented for several industrial electronics assemblies, which are complex 3D setups with realistic physical parameters, to enable automatic and more efficient design optimization using surrogates compared to brute force search.

2 Physics Informed Neural Networks (PINNs)

2.1 Physics informed Neural Networks

Proposed by Raissi et al. [49], physics-informed neural networks (PINNs) leverage automatic differentiation to obtain an analytical representation of an output variable and its derivatives, given

a parametrization using the trainable weights of the network. By employing the underlying static graph it is possible to construct the differential equations that govern physical phenomena. Using gradient-based optimization the residual is converted into a loss function and driven to zero in order to satisfy the PDE. Similarly, the same methods can be used for the boundary conditions (Dirichlet/Neumann/Robin) and initial conditions to completely construct a well-posed PDE for the neural network to solve.

Once the static graph for PINN training has been created, any iterative gradient-based optimization algorithm can be used to minimize the loss function. Popular choices in literature, include Adam [30] and L-BFGS. Both these optimizers come with advantages and drawbacks. For smaller problems, a combination of Adam followed by L-BFGS to fine-tune the optimization works well. However, for larger problems, the full batch size requirement of the L-BFGS second-order optimizer limits its use to small/simplified problems.

Theoretically, PINNs require no data to train since the loss function will contain all the terms necessary to completely describe the PDE problem. However, depending on the implementation, they may require training data. If the objective is to do a forward solve (i.e solving for the solution of the PDE), no data should be required. If, however, one is solving an inverse problem (i.e given some/all of the solution and part of the PDE infer the rest of the PDE), they will need some training data and the known part of the PDE. This diversity in potential applications is where the true potential of PINNs lies; PINNs represent the intersection of PDE-based and data-driven solution methods for systems that can be described by partial differential equations, in a very simple, efficient manner. They allow for the creation of models that, if trained correctly, increase the likelihood that the models will obey the PDE-based laws of physics as applicable to the processes they are modeling. Even in cases where PINNs cannot be trained correctly in a data-free manner (described in Section 3), including the physics as an inductive bias has been shown to improve the surrogate models by reducing overfitting and making the results more physical [34, 65].

2.2 Mathematical Formulation

A PDE problem in the general form reads:

$$\mathcal{N}_{\mathbf{x}}[u] = 0, \mathbf{x} \in \Omega,$$

$$u(\mathbf{x}) = g(\mathbf{x}), \mathbf{x} \in \partial\Omega.$$

In order to solve the PDE using the PINN method, the residual of the governing PDE is minimized, which is defined by

$$r_{\theta}(\mathbf{x}) = \mathcal{N}_{\mathbf{x}}[f_{\theta}(\mathbf{x})],$$

where f_{θ} is the predicted value by the network. The residual value, along with the deviation of the prediction from boundary/initial conditions, is used to construct the loss, which takes the form:

$$L(\theta) = L_r(\theta) + \sum_{i=1}^M \lambda_i L_i(\theta),$$

where the index i refers to different components of the loss function, relating to initial conditions, boundary conditions and measurement/simulation data. λ_i refer to the weight coefficient of each loss term. The individual loss terms are constituted as follows:

$$\begin{aligned} L_r &= \frac{1}{N_r} \sum_i^{N_r} [r(\mathbf{x}_r^i)]^2, \\ L_b &= \frac{1}{N_b} \sum_i^{N_b} [u(\mathbf{x}_b^i) - g_b^i]^2, \\ L_d &= \frac{1}{N_d} \sum_i^{N_d} [u(\mathbf{x}_d^i) - \hat{u}(x_d^i, t_d^i)]^2, \end{aligned}$$

where the subscripts r,b,d refer to collocation, boundary, initial and data points, respectively.

2.3 Current Challenges with PINNs

Although the PINN method shows great promise, it still has a number of unresolved issues. The biggest challenges with PINNs currently lie in the scalability of the algorithms to large 3D problems as well as problems with complex nonlinearities, and unsteady problems.

2.3.1 Weak imposition of Boundary Conditions

The solution of a PDE problem must obey all initial and boundary conditions imposed on it while minimizing the residual of the governing equation. However, for neural network based solvers it is difficult to impose boundary and initial conditions in an exact manner. This is because the standard way to impose B.C in PINNs is to create a linear combination of loss functions (as described mathematically in the previous section). Each loss either describes the deviation of the network output from a specific boundary condition, or the magnitude of the residual of the governing equations. Therefore, boundary conditions are only satisfied in a weak manner. There has been research demonstrating the utility of exact imposition of boundary conditions [38, 59, 60] or creative multi-network approaches [52], such implementations are mostly problem-specific and do not generalize well.

Weak imposition of boundary conditions also creates another issue, one that is fairly common in multi-task learning and multi-objective optimization: choosing the values of loss term coefficients that make up the linear combination. Choosing these weights is a nontrivial exercise that would require calibration via hyper-parameter search, which is not feasible. Wang et al. [64] introduced a heuristic dynamic weighting algorithm to update and select these weights automatically and continuously during the training, to enable convergence to the correct answer. Additionally, there have been several other algorithms proposed to choose the correct scheme for weighting the losses [5, 67, 68]. This continues to be an active area of research in the PINNs community. Finally, methods have been proposed to impose the boundary conditions in a strong manner by manipulating the output formulations [60] or by utilizing operator networks [53].

2.3.2 Difficult Optimization Problem

A second problem is the nature of the loss landscape itself, in which a reasonable local minimum is required to be found. As seen in Krishnapriyan et al. [33], Gopakumar et al. [21], Subramanian et al. [58] and Basir and Senocak [2], as well as the author’s own experiments, different non-dimensional quantities (e.g. Reynolds number) in the governing equations, the number of dimensions of the problem, the point cloud/discretization, the boundary conditions and the complexity of the solution to be predicted can adversely affect the loss landscape of the neural network training. This makes the optimization challenging and can fail to find an adequate local minimum via a gradient descent-based algorithm. Recently, methods borrowing concepts from optimization theory have shown alternate formulations (e.g. augmented lagrangian method for the loss functions) can aid the convergence properties of the training problem [2, 57]. There have also been efforts towards imposing physical constraints in an integral form [23].

2.3.3 Cost of training

Constructing the PDE loss functions involves several backward passes through the network, which is a costly operation. PINNs on average takes longer to train than their data-driven counterparts for exactly this reason; the computation graph of a PINN training is much more complex. Moreover, for the Navier-Stokes equations, it has been seen that although the stream function formulation provides better results (due to exact enforcement of continuity), it is costlier in terms of training time. As seen in NVIDIA’s experiments [25], it can take several million iterations for the more complex problems to be solved via PINNs. To reduce the cost of training approaches such as automatic differentiation for finite difference formulations [24], or using first-order formulations [18], have been proposed. However, these solutions tend to be mostly problem-specific and do not necessarily generalize well to increased problem complexity and grid definitions. Meta-learning algorithms [16] have also recently gained significance as an effective way to reduce the cost of training neural networks on new tasks, and some of this work has been extended to PINNs [46] as well.

2.3.4 Unsteady problems

As discussed above, in a standard implementation, solving a time-dependent problem via PINNs is a challenging task. This is primarily because the standard implementation treats time as another axis just like space; what this means is that in creating the spatial point discretization, the space mesh has to be repeated for every time step. This can be a very expensive process for any problem except simple 1D and 2D problems. Moreover, another very important issue with this method is the lack of respect for causality. It was demonstrated by Wang et al. [66] that networks have a tendency to learn the solution of the PDE at later time steps first, and if the solution does not correctly solve for earlier time steps, the solution at later time steps will most likely be incorrect. In literature, a number of methods have been proposed to get around these issues [6, 33]. Krishnapriyan et al. [33] suggests using a sequential model approach, breaking down the total set of time steps into blocks of consecutive steps. Each block of time steps has its own dedicated trained model, using either the initial condition provided (with the PDE to solve) or the solution of the previous block of time steps as the initial condition for the next block's neural network solve. This approach has been shown to lend stability to the training, as occasionally trying to solve for all time steps simultaneously would fail. However, the bigger benefit for simulating industry-grade problems, which have larger meshes/point clouds, is that with this breakdown of the problem, the training for each network that represents a sub-block can be fit on a GPU. These networks can then be trained in a sequential manner, much faster on a GPU as compared to a CPU. To address the problem of causality, Wang et al. [66] suggested a dynamic weighting approach for the loss terms corresponding to each time step that would favor the network learning the solution in a causal manner.

Another way of solving time-dependent problems using PINNs, is to use layers that were designed to deal with sequential data in the first place. In conventional data-driven deep learning, for applications like time-series analysis and natural language processing, RNN and LSTM layers were designed to deal with sequences of data instead. For applications in scientific machine learning, these layers can be adapted to deal with time sequences. Work by Wu et al. [69] and Cheng et al. [12] has already demonstrated promising applications of these layers to scientific ML.

3 Important Features

In this section, some of the important features used in the framework are outlined for the creation of ANN-based surrogate models.

3.1 Fourier Feature Embeddings

As described in Tancik et al. [62], Artificial Neural Networks suffer from a spectral bias problem. To overcome this, they introduced a Fourier feature embedding that allows models to capture high-frequency components of the solution effectively. In addition, there have been other proposed solutions for the spectral bias problem for applications to PDE problems, such as the Siren activation [56], Fourier Neural Operators [35], and weighting schemes derived from the theory of Neural Tangent Kernels (NTK) [68].

3.2 Embedding Physics as an Inductive Bias

It is clear that the current state of the art in PINNs has improved the method significantly from what was proposed in the first paper [49], and researchers have been able to gradually solve PDE-based problems involving more complex nonlinearities and in more dimensions. However, the PINNs method is currently not suited for solving complex engineering problems often encountered in industry in a data-free manner. The optimization issues and cost of model training outlined above make the method, presently, unsuitable for use as a forward solver. To get the best of both worlds, the PINNs method can be augmented with data. Figure 1 depicts the tradeoff between using only data or only physics, and that the sweet spot lies in using both. There have been several examples showing that the inclusion of solution data significantly improves the convergence capabilities of the method [8, 9, 54]. This has a number of distinct advantages:

1. The combined data-physics approach can be used to solve ill-posed problems (for example, problems with missing B.C that have some solution data available)
2. Create surrogate models using lesser solution data that are more consistent with physics and hence more accurate [1, 34, 65]
3. Inverse problems for system identification [27, 70]

The simplicity and non-intrusiveness of the method allow a user to quickly set up a problem on top of a standard solver.

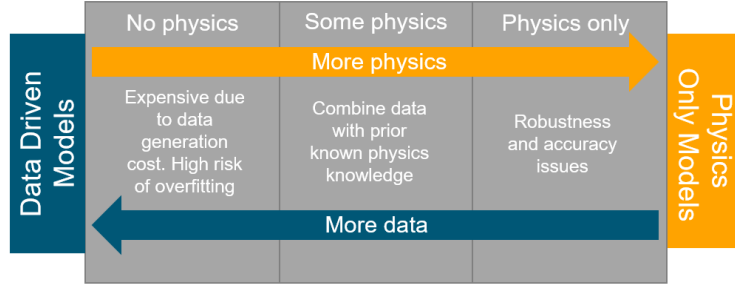


Figure 1: The spectrum of data-driven versus physics-informed models. Incorporating governing physics information into the models during creation serves as an effective form of regularization and often helps reduce the amount of data required to achieve the same accuracy levels

3.2.1 Demonstration

To demonstrate the effect of adding physics-based regularizers to the training and their effect on the final converged solution, a comparison of data versus data plus physics was undertaken. In this experiment, a coarse selection (1% of the total nodes) of points was selected randomly to use for the data term; all nodes were used for the physics. Since the mesh had approximated 230,000 node points, this meant 2,300 data points. The experiment is divided into two parts, first, a model is trained on this 1 % data without any physics, and then a new model is trained starting with 1 % data and then adding the physics at all nodal points (using a warm start approach described in Section 3.4). To the author's knowledge, this represents a novel attempt at using a very coarse solution to aid convergence of the network to physically correct solutions in 3D for an external flow at a high Reynolds Number. This class of problem is conventionally challenging for PINNs due to the nonlinearity and gradients involved.

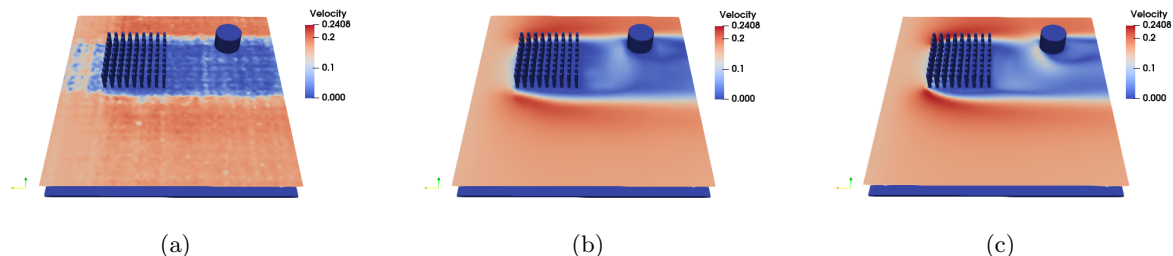


Figure 2: ANN prediction with and without physics, for very coarse data supplied. (a) Trained on 1% solution data from solver (b) Trained on 1% data and physics (c) True Solution from CFD solver

Figure 2 shows the ANN predictions for different case results. It is evident that by using sparse data, the network is able to converge to the right answer using the physics-based regularizer. It should be noted that the eddy viscosities are provided at each node point in this example, to the physics residual. However, this opens exciting possibilities about using physics-based regularizers in the future. Data generation costs to create surrogate models can be greatly reduced by providing solution data on a very

coarse grid and solving the physics on a much finer grid. This has been demonstrated by Gopakumar et al. [21] for 2D flow over a block. Ghosh et al. [17] also uses sparse solution data in the domain to create surrogate models for flow over a cylinder at high Reynolds number in 2D.

It should be noted that the above result was demonstrated using a small fraction of overall solution data to show the effect of adding physics. In the rest of the paper, wherever a data term was used for training, all available training data for a set of input parameters was used.

3.3 Domain Decomposition

The domain decomposition process is defined as breaking the overall solution domain into several subdomains and defining a model for each subdomain. As discussed by Jagtap et al. [28] and Hu et al. [26], breaking down the overall solution domain into subdomains can allow for better generalization capability for complex multiphysics and multiscale problems since predictions for each subdomain are performed on the sub-network of that domain. Furthermore, the training of sub-networks obtained via domain decomposition is inherently parallelizable and the sub-domain models can be placed on separate GPUs with an associated speedup. Care must be taken as mentioned by Hu et al. [26] to avoid overfitting the model.

3.4 Warm Start for Physics

One of the issues with using standard initialization schemes like Xavier [19] for training a PINN in a data-free manner, is that the resulting outputs of the networks have no physical meaning at the start of the training. Minimizing residual-based losses, in this case, is very ineffective since the gradients generated by backpropagation are likely to be very noisy and increase the likelihood of the training converging to a bad local minimum. One solution is to have a "warm start" by first training on some solution data only. This has two benefits:

1. It brings the network weights closer to their "converged" values before using the PDE residuals to improve the quality of the solution generated by the network. This allows the PDE residuals to be much more effective in the training process.
2. It reduces the cost of training. As discussed in Section 2.3.3, computing gradients of PDE residuals via backpropagation is an expensive operation. By using a warm start via a pretraining approach, one can mitigate this cost by avoiding training iterations where the physics would have little to no benefit on the training process.

4 Implementation

4.1 Model Setup

A simple fully connected architecture with 3 hidden layers of 128 nodes each for fluid domains, and 2 hidden layers of 64 nodes each for solid domains were used. This distinction was made because of multiple reasons:

- The solution in the fluid subdomains is likely to be much more non-linear, particularly in regions of fine sampling like the boundary layer. Hence a smaller network can be used for the thermal subdomains as solutions in these subdomains are not likely to require as much expressive power.
- A flow-thermal domain is likely to have more thermal subdomains than fluid subdomains. This can be seen in the example on the electronics box (Section 5.2.3) where there is 1 flow subdomain and 27 thermal subdomains. In the interest of cost-effectiveness from a computing perspective, smaller networks are used to express the solutions in solid domains where only the energy equation is being solved.

In addition, the space coordinates are encoded in the frequency domain as described in [62]. The number of outputs of the network depends on the governing equation. For the Navier Stokes Equations, there are four outputs (u, v, w, p), and for the energy equation, there is one output (T). The number of inputs to the network depends on the number of axes of parametrization for the given problem. For

example, if the parametrization is along one axis (say Re) then the total number of inputs would be 4 (3 spatial + one parameter). This network architecture is not the result of a parameter search. The model is trained using an ADAM optimizer. The framework also supports using L-BFGS, however, it is only recommended to use L-BFGS with full batch size; this is problematic from a memory perspective for 3D nonlinear problems.

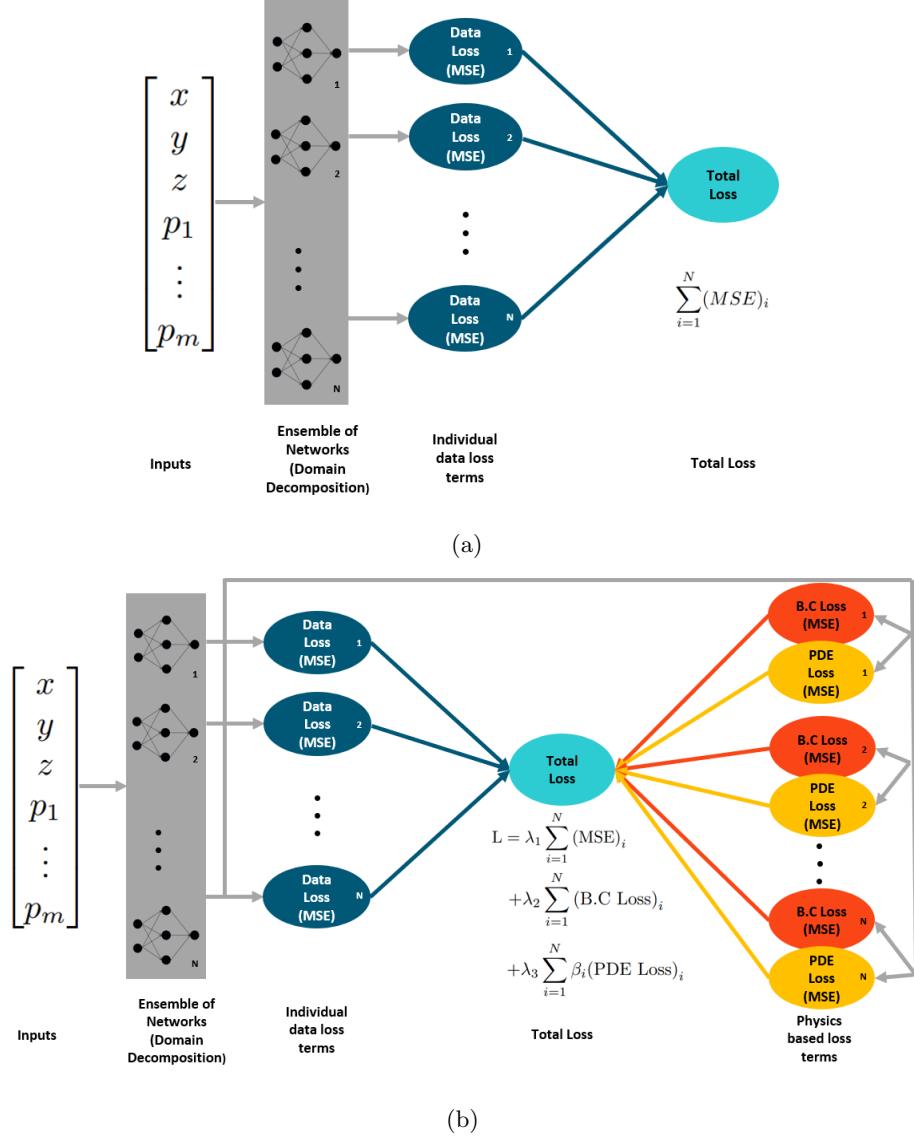


Figure 3: Training graphs during different training phases. (a) Training graph for warm start (b) Training graph when physics is included

The training process for a surrogate model can be divided into two phases, depicted in Figures 3a and 3b. The input vector to any of the N sub-networks is the coordinates and the input parameter set of m parameters (if creating a surrogate model). For the training warm-up (described in Section 3.4), only the solution data loss is included in the total loss, referenced in Figure 3a. Once the warm-up is complete (based on a fixed number of iterations or convergence criteria), include the physics-based losses to enhance the training (shown in Figure 3b). For the case with multiple sub-domains, the PDE losses are scaled relative to one another at the start of the training as follows:

$$\beta_i = \min\left(\frac{\max_{i=1,\dots,N} (PDE \text{ Loss})_{i,iter=0}}{(PDE \text{ Loss})_{i,iter=0}}, 10^5\right),$$

The outer min is added to avoid exploding gradients due to very high coefficients. The inter loss

coefficients λ_i are determined using Learning Rate Annealing [64].

4.2 Design Optimizer Setup

To optimize physical designs with trained models that predict flow-thermal results, the Particle Swarm Optimization (PSO) [29] algorithm is used. It is a zero-order optimization method that uses an initial distribution of particles in the search space and based on the "fitness" of each particle computes new positions and velocities of particles in the search space. Eventually, the particles converge towards the optima.

The current categories of problems being solved in this paper (i.e constrained flow-thermal design optimization problems) take the general form

$$\begin{aligned} & \min_{\mathbf{u}} f(\mathbf{u}), \\ \text{s.t.} \\ & g_i(\mathbf{u}) \leq X_i \quad i = 1 \dots N, \\ & u_j^{\min} \leq u_j \leq u_j^{\max} \quad j = 1 \dots M, \end{aligned}$$

where f represents an objective function, g_i represents the i th constraint and X_i represents constraint values. \mathbf{u} represents the input vector of design parameters (of length M), and each component of \mathbf{u} has a u_j^{\min} and u_j^{\max} that they can take. The objective and constraint values would be a derivative of flow thermal variables like pressure, temperature, or velocities, or design variables like geometry lengths, inflow rates, or source terms. The objective and constraints can be placed on bodies, individual surfaces, or the internal volumes of components that are a part of the simulation.

In order to solve this problem via the PSO algorithm, the constrained optimization problem is converted to an unconstrained problem via the penalty method to get the objective function:

$$f(\mathbf{u}) + \sum_{i=1}^N \lambda_i \cdot (g_i(\mathbf{u}) - X_i)^2 \cdot \mathbb{1}(g_i(\mathbf{u}) > X_i) + \beta \sum_{i=1}^N \mathbb{1}(g_i(\mathbf{u}) > X_i).$$

The first term is the constrained objective function. The second term represents the degree of deviation of the constraint from the boundary if the constraint is violated. The third term adds cost based on the number of constraints violated, and λ_i and β are constants.

Once the objective function is set up, the i th particle positions (\mathbf{u}) and velocities are updated according to the equations

$$\begin{aligned} \mathbf{u}^i &= \mathbf{u}^i + \mathbf{v}^i, \\ \mathbf{v}^i &= w\mathbf{v}^i + c_1 r_1 (\mathbf{u}_{best}^i - \mathbf{u}^i) + c_2 r_2 (\mathbf{u}_{best} - \mathbf{u}^i), \end{aligned}$$

where c_1, c_2, r_1, r_2 and w are constants.

There are several reasons why PSO is chosen for design optimization:

1. It is more economical to use compared to brute force grid search of Design of Experiment (DoE) space via querying solutions from the ANN. While this may not seem intuitive, in cases where there is pre-processing required (of say the point cloud) before the ANN can be queried for the result, It helps to minimize the amount of computation required. An example of this is when parametrizing geometry, in which case to query a new \mathbf{u} a new points cloud/mesh would have to be generated.
2. The distribution of particles at convergence gives a smaller subspace to do high-fidelity modeling, rather than returning a single particle as the best solution. This is important because the modeling process via ANNs is not exact or high fidelity, and it is better to have a subset of the DoE space returned rather than a single point, as for example, a gradient-based optimization method may do. Moreover, there may be multiple regions of the DoE space which satisfy the constraints and minimize the objective, and the PSO method can return both regions

Figure 4 depicts the design cycle using the PSO algorithm. In traditional design optimization, Step 1 is done using CFD solvers, but this can get very expensive. NN-based surrogates are an ideal tool to replace CFD solvers for early-stage design cycles.

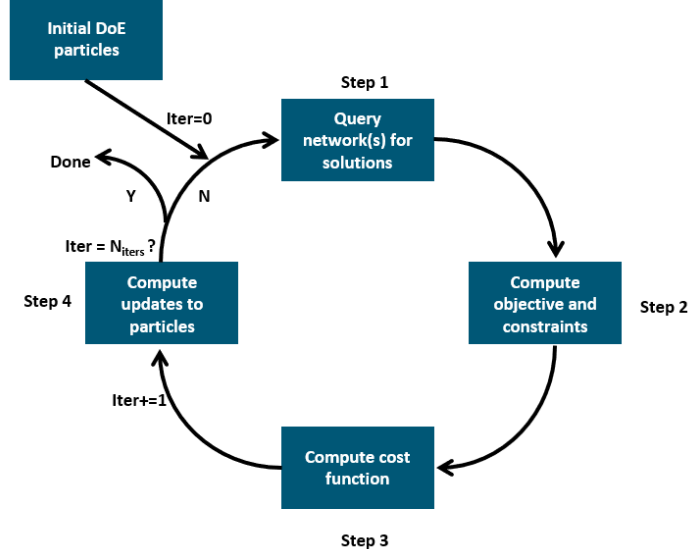


Figure 4: A design iteration using a design optimization algorithm (like PSO)

5 Applications

5.1 Forward Solve of 3D Stenosis Problem

As a first step to demonstrate the solver/surrogate modeling framework, flow through an idealized 3D stenosis geometry at a physiologically relevant Reynolds number is demonstrated, see Figure 5 for details about the geometry. To the author's knowledge, flow through a stenosis has been solved using PINNs only at a low Reynolds number of approximately 6 (based on inlet diameter) [60]. Flow through irregular geometries has been solved at a higher Re (500), but in 2D [44]. In this paper, the stenosis problem is solved at Re 150, and in 3 dimensions. As pointed out by Krishnapriyan et al. [33], at higher Reynolds numbers the standard PINN implementation struggles to achieve a good local minimum. This was confirmed using a standard PINN implementation. To alleviate this issue, there are several approaches that can be taken. First, sporadic solution data can be added throughout the domain of interest (depicted in Figure 6b). Tests confirmed that this significantly reduces convergence time and allows us to arrive at the correct solution in complex domains. Second, as proposed by NVIDIA continuity planes can be used to enforce mass/volume flow rate conservation across the cross-section of internal flows [25] (depicted in Figure 6a). This was implemented in the framework, using basic Euler integration to solve for the mass flow through a cross-section based on the inlet mass flow rate.

5.1.1 Problem Setup

The flow problem through the stenosis is solved by solving the steady-state Navier-Stokes equations:

$$\nabla \cdot \mathbf{u} = 0,$$

$$(\mathbf{u} \cdot \nabla) \mathbf{u} = -\frac{1}{\rho} \nabla p + \nu \nabla \cdot (\nabla \mathbf{u}),$$

subject to

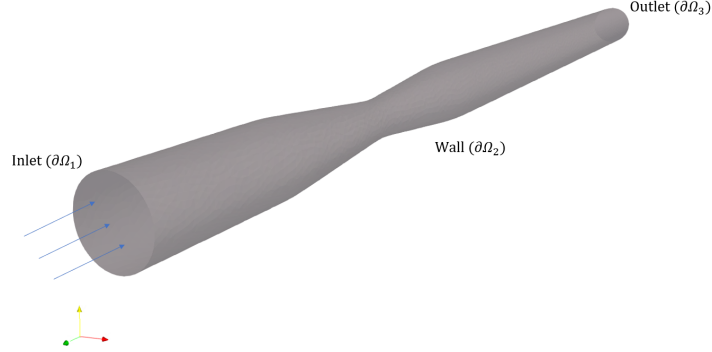


Figure 5: Visual description of stenosis problem

$$\mathbf{u}(x_{b1}) = 0, x_{b1} \in \partial\Omega_2,$$

$$\nabla u_i(x_{b2}) \cdot \mathbf{n} = 0, x_{b2} \in \partial\Omega_3, i = 1, 2, 3,$$

$$\mathbf{u}(x_{b3}) = g(x_{b3}), x_{b3} \in \partial\Omega_1,$$

where $g(x_{b3})$ represents a profiled input to the stenosis.

In the present problem, a parabolic profiled input is provided with a peak value inflow of 0.15 m/s. The ratio of areas of the throat to the inlet is 0.36.

The output of the network is approximated as G_θ , which is a 4-component output, and use the network output to estimate all 4 components of the output:

$$u = G_{\theta,1},$$

$$v = G_{\theta,2},$$

$$w = G_{\theta,3},$$

$$p = G_{\theta,4}.$$

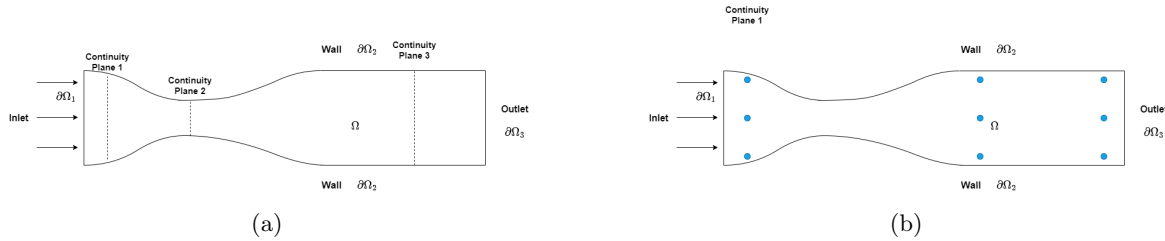


Figure 6: Slices of stenosis showing several ways of aiding PINN convergence (a) Positions of continuity planes (b) Position of solution data provided

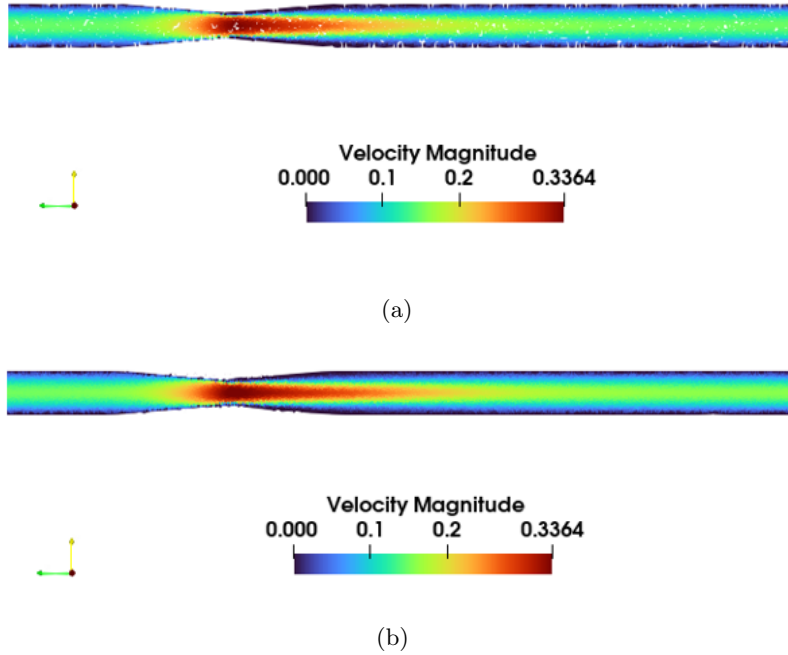


Figure 7: Solution Comparison. (a) Altair AcuSolve® Solution to stenosis problem (b) PINN forward solve to stenosis problem.

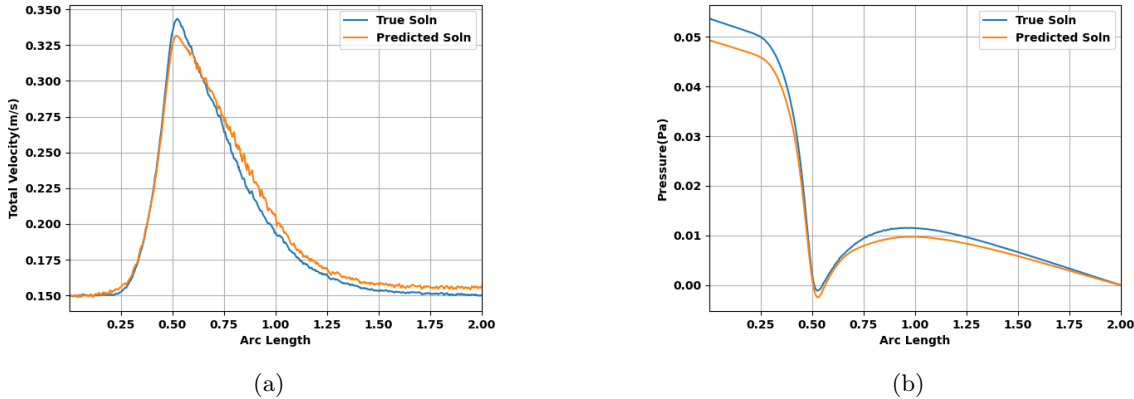


Figure 8: Centerline solution comparisons : PINN versus Altair AcuSolve® (a) Total Velocity Comparison (b) Pressure Comparison

5.1.2 Results

Figure 7 compares the velocity magnitude returned by the trained PINN model and Altair AcuSolve® through a 2D slice of the stenosis. As can be seen, the essential features of the flow are captured. Figure 8a and 8b compare the velocity and pressure profile through the center of the stenosis. The differences between the line plots are attributed to differences in mesh fineness between the two cases. It should also be noted that making minor adjustments to the fineness of sampling of the continuity plane affects the solution from the PINN.

5.2 Surrogate Modeling and Design Optimization

In the following subsections, the PINNs surrogate modeling technique is demonstrated for rapid design iteration in the electronics cooling space. Three key ideas are combined in this approach: data-

driven modeling; physics-informed methods; and optimization algorithms (see section 4.2). For the data enhancement, sampling of FE data on a coarse DoE space is undertaken. The physics-informed nature comes about through the inclusion of a PDE-based regularizer as previously discussed. The combination of these two methods allows both accuracy and robustness (as discussed in Section 3.2).

5.2.1 Heat Sink Design Optimization

The electronics assembly utilizes a chip with a fin-type heatsink on top to dissipate heat into the surrounding fluid. The chip-heatsink assembly is cooled by forced convection of air. The geometry and setup are shown in Figure 9. The governing equations solved for this conjugate heat transfer problem are, the Navier-Stokes for the flow domain surrounding the chip-heatsink assembly:

$$\nabla \cdot \mathbf{u} = 0,$$

$$(\mathbf{u} \cdot \nabla) \mathbf{u} = -\frac{1}{\rho} \nabla p + \nu \nabla \cdot (\nabla \mathbf{u}),$$

subject to no-slip boundary conditions on the surrounding box and on the chip-heatsink assembly with a variable velocity at the inlet. The energy equation in both fluid and solid reads:

$$\nabla^2 T + \dot{q}_{src} - \mathbf{u} \cdot \nabla T = 0,$$

where the velocity is zero in the solid. At the interface between the fluid and solid domain (fluid-sink, sink-chip, and fluid-chip) the interface condition is applied by minimizing the following loss terms as shown in [28]:

$$L_{flux} = \frac{1}{N_{int}} \sum_{i=1}^{N_{int}} (f_{d_1}(\mathbf{u}(x_i)) \cdot \mathbf{n}_{d_1} + f_{d_2}(\mathbf{u}(x_i)) \cdot \mathbf{n}_{d_2})^2,$$

$$L_{val} = \frac{1}{N_{int}} \sum_{i=1}^{N_{int}} (\mathbf{u}_{d_j}(x_i) - \overline{\mathbf{u}_{d_j}(x_i)})^2,$$

where $\mathbf{n}_{d1} = -\mathbf{n}_{d2}$ and $j=1,2$. The average is taken over j . d_1 and d_2 refer to the domains on both sides of the interface, and N_{int} is the number of node points on the interface.

The goal of the heatsink optimization is to find the maximum power the chip can generate subject to certain constraints.

The design variables that can be altered for this present optimization are:

- Inflow Velocity
- Fin height
- Source term in the chip (has to be maximized)

The upper and lower limits of each of the design variables mentioned above are summarized in Table 1. The inlet velocity is set based on typical values found in literature [36] and corresponds to a Reynolds number range of Re 10,300 to Re 24,000. The domain is divided into three parts (Fluid,

Parameter	Lower Value	Upper Value
Inflow Velocity (m/s)	3	7
Fin Height (mm)	15	23
Source Term (W)	30	60

Table 1: Design of Experiments space axes ranges for the heat sink design optimization

chip and sink) and each part has its own prediction network. The material properties were as follows: Chip is made of FR-4; Heatsink is made of Aluminium; and the cooling fluid is air. The material properties are shown in Table 2

Domain	Density (kg/m^3)	Dynamic Viscosity(kg/ms)	Conductivity(W/mK)	Specific Heat(J/KgK)
Chip	7190.0	-	50.208	460.0
Sink	2770.0	-	175.0	986.0
Air	1.225	1.78 e-5	0.0251	1006.0

Table 2: Physical properties of different subdomains in the heat sink design optimization

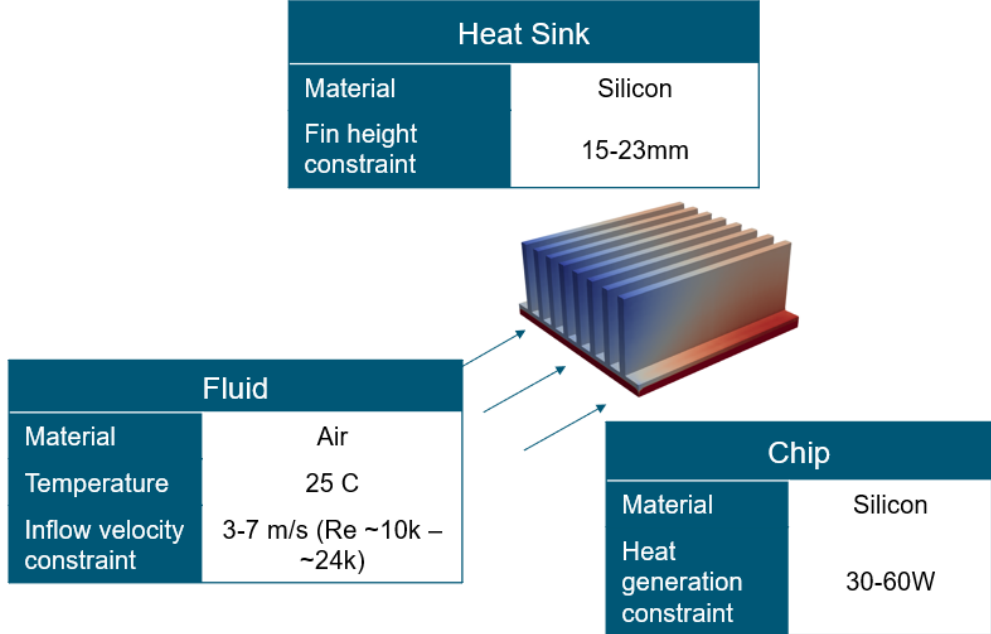


Figure 9: Basic problem geometry and flow depiction

The Model Creation Process

The sampling of the above Design of DoE space is done via an efficient space-sampling method to optimally fill the DoE space [41]. Sampling strategies are important to minimize the number of samples while keeping the design exploration process accurate and simultaneously cost-efficient. The model was trained on a single Titan V GPU card, on which the overall training time was around 130 mins.

The Optimization Process

In order to optimize designs based on user-defined constraints, the created surrogate models are interfaced with an optimizer that solves a generic constrained optimization problem, described in section 4.2. The same is demonstrated in the example case:

$$\begin{aligned} \text{Pressure drop across the heat sink channel} &\leq 11 \text{ Pa} \\ \text{Maximum temperature anywhere on the chip} &\leq 350 \text{ K} \end{aligned}$$

Each snapshot in Figure 10 represents a design iteration, and each particle represents a point in the DoE space. Each axis of a plot represents a parameter axis.

For the given constraints, the particles converge to a much smaller region of the DoE space. Due to imperfections in the overall modeling process, the aim should not be to return a single design point to the user but a massively truncated DoE space in which they can then run high-fidelity CFD to optimize their design. For the sake of demonstration of results, however, a single point in this truncated DoE space is chosen. The design point returned by the optimizer in this case is:

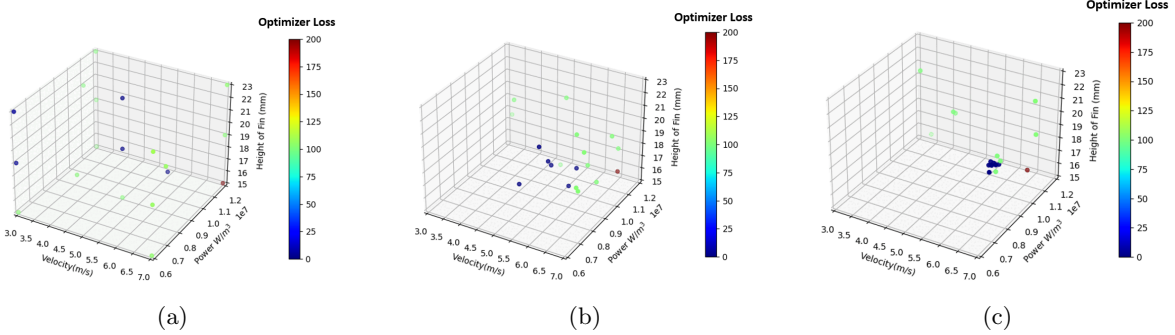


Figure 10: Design optimization iterations of the heat sink problem (a) Iteration 0 (b) Iteration 5 (c) Iteration 10

Inflow Velocity: 6 m/s
Chip Power: 50W
Fin Height: 17mm

To test the result, high-fidelity CFD of the problem is run at the above design point and compared to the result from the framework. As shown in Figures 11 and 12, not only are the differences in solution minimal, but the given design point nearly satisfies the design constraints. The time taken for the overall design optimization after model training was 10 minutes, and this approach shows how effective surrogate modeling-based optimization approaches can be in reducing turnaround times for design problems. The resultant best parameters can hence be tweaked a little by using high-fidelity CFD to obtain a satisfactory design.

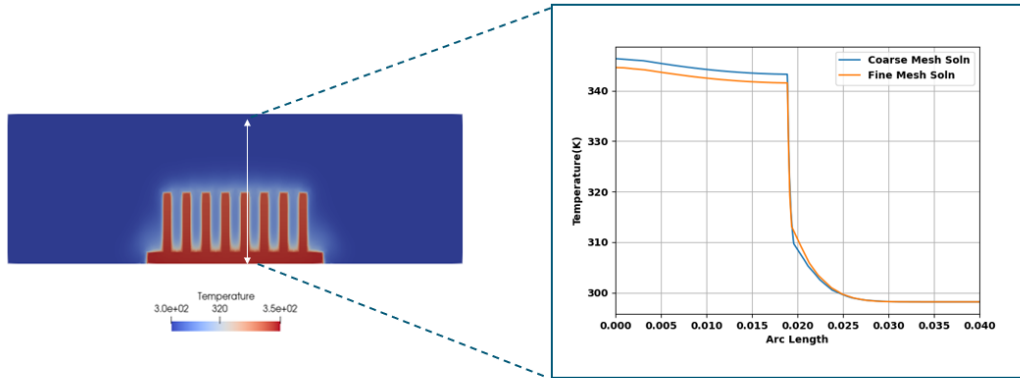


Figure 11: Temperature plot through a slice at the rear of the sink (from bottom to top). The comparison between the high-fidelity solution on the fine mesh and the PINN prediction on a coarser mesh shows good agreement

5.2.2 Printed Circuit Board Thermal Analysis

In this example, thermal analysis of a PCB board and its components is done. The setup is shown in Figure 13, with the material properties of the components described in Table 3. The value ranges for each axis of the DoE is shown in Table 4. The goal is to compare the solution from the ANN surrogate to the solution from the CFD solver and test the ability of the model to generalize to new test points. After that, a similar optimization problem to the previous section is solved. The physics of the problem is identical to that of the heat sink design problem and is not described again for brevity.

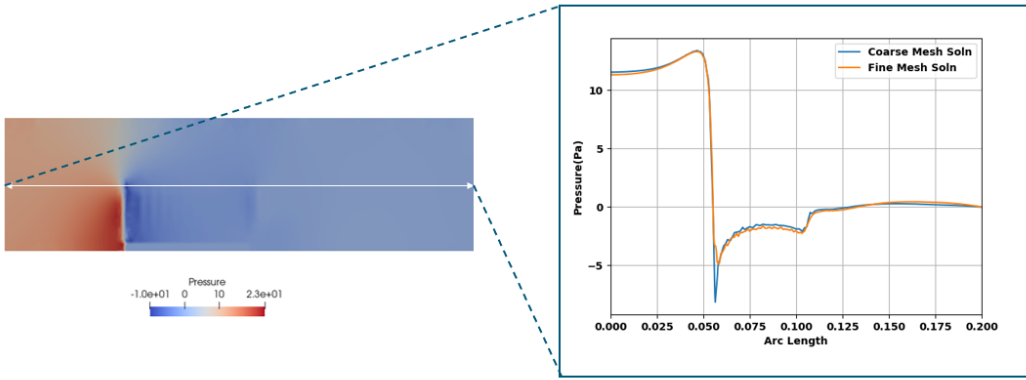


Figure 12: Pressure plot through a slice through the middle of the flow channel (from left to right). The comparison between the high-fidelity solution on the fine mesh and the PINN prediction on a coarser mesh shows good agreement

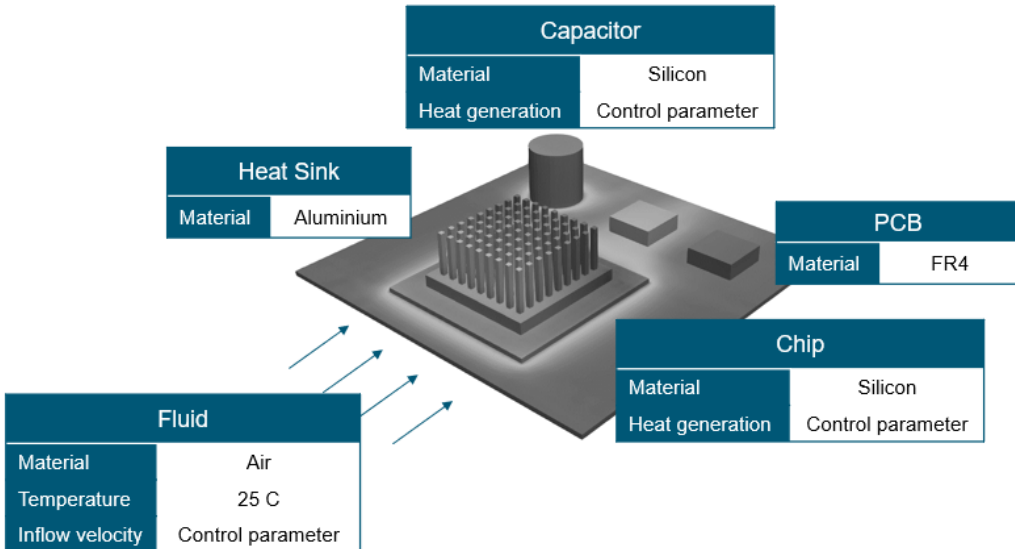


Figure 13: Basic problem geometry and flow depiction

Domain	Density (kg/m^3)	Dynamic Viscosity(kg/ms)	Conductivity (W/mK)	Specific Heat (J/KgK)
Air	1.225	1.78 e-5	0.0251	1006.0
Capacitor	700.0	-	82	2330.0
Chip	700.0	-	82	2330.0
Sink	2770.0	-	175	986.0
PCB	1850	-	0.294	1900.0

Table 3: Material Properties for PCB analysis problem

The Model Creation Process

The sampling of the above DoE space is done via an efficient space-sampling method, to minimize the number of samples required to fill in the DoE space in an efficient manner. 8 data points are used for the model creation process. The model was trained on a single Titan V GPU card, on which the overall training time was 100 mins. The total time taken to generate the model was around 120

Parameter	Lower Value	Upper Value
Inflow Velocity (m/s)	3	9
Source Term(Chip) (W)	30	100
Source Term(Capacitor) (W)	3	10

Table 4: DoE parameter ranges for PCB analysis problem

minutes (including data generation time, done on a highly efficient 32-core cluster).

Results

Prediction versus truths for 2 line plots for two randomly selected test points (far enough from any training points) within the DoE space as defined above. The two lines were chosen to get a quantitative comparison between results while capturing the relevant physics. Though only results for energy equation solves were shown, the model trained was a flow-thermal one.

Parameter set 1

- **Inflow Velocity:** 5 m/s
- **Thermal Power in Chip:** 90 W
- **Thermal Power in Capacitor:** 10 W

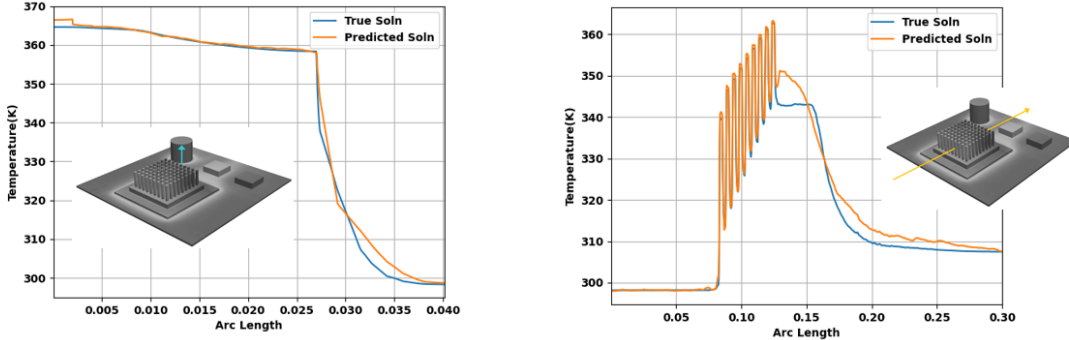


Figure 14: Line plot results for Parameter Set 1: CFD prediction versus Network Prediction

Figure 14 compares the Altair AcuSolve[®] and ANN solution through two lines. The left figure captures the solution in a fin of the sink, in a region that is the hottest during the operation of the chip. The right figure captures the temperature in the streamwise direction. The solutions for this test case show good agreement, except for the wake area behind the sink. This is attributed to imperfections in the flow solution in the wake of the sink.

Parameter set 2

- **Inflow Velocity:** 8 m/s
- **Thermal Power in Chip:** 50 W
- **Thermal Power in Capacitor:** 5 W

Figure 15 again compares the Altair AcuSolve[®] and ANN solution through two lines. The solutions for this test case also show good agreement, with some deviation in the wake of the sink.

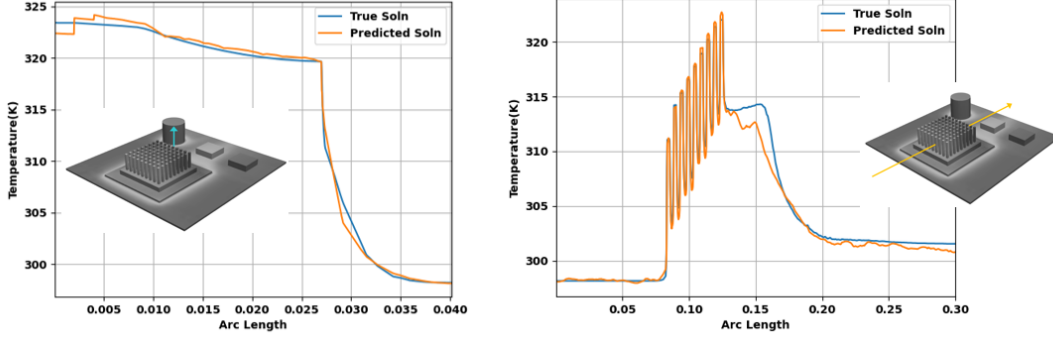


Figure 15: Line plot results for Parameter Set 2: CFD prediction versus Network Prediction

Design Optimization

The optimization feature of the framework is used to solve a similar design optimization problem as before. One example problem is as follows:

$$\begin{aligned}
 & \text{Maximize } Q_{chip} \text{ s.t} \\
 & \text{Pressure drop across channel} \leq 20 \text{ Pa} \\
 & \text{Maximum Temperature in Chip} \leq 340 \text{ K} \\
 & \text{Maximum Temperature in Capacitor} \leq 340 \text{ K}
 \end{aligned}$$

This makes for an interesting optimization problem as there is a slight interaction between the wake of the chip and the capacitor

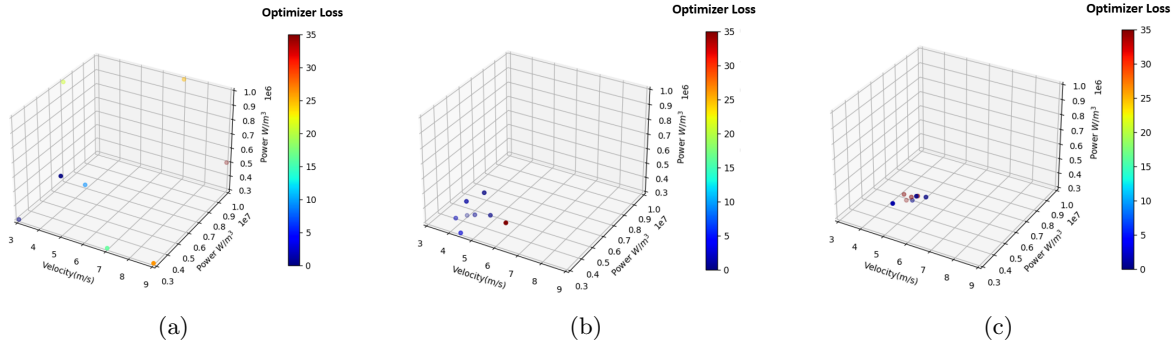


Figure 16: Design optimization iterations of the PCB design problem (a) Iteration 0 (b) Iteration 5 (c) Iteration 10

Figure 16 shows the PSO algorithm converging to the best region of the DoE space, which satisfies the constraints and solves the optimization problem. Although the purpose of the optimizer is not to return a single point but to return a truncated DoE space, for argument's sake a single returned point, which has the parameters:

$$\begin{aligned}
 & \text{Inflow Velocity: } 5.5 \text{ m/s} \\
 & \text{Chip Source Term: } 5.5 \text{ e6W/m}^3 \\
 & \text{Capacitor Source Term: } 3.87 \text{ e5W/m}^3
 \end{aligned}$$

The returned answer is compared to the CFD result at this optimal point. Looking at the constraints defined above, it is visible in Figure 17 that the surrogate-optimizer combination has very efficiently returned an optimal operating point that maximizes the utilization of the chip (and the thermal power dissipated).

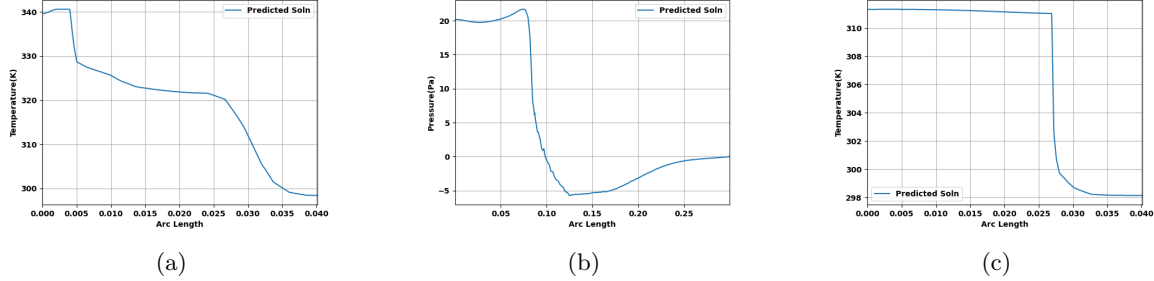


Figure 17: Checking values of physical variables in solution domain to see if they satisfy constraints. (a) Start of the plot indicates the temperature in the PCB followed by chip (b) Pressure across flow channel. Left end shows pressure at the inlet (c) Temperature through the length of the capacitor

5.2.3 Electronics Box Analysis

Finally, the ability of the framework to model the flow thermal characteristics of an entire electronics box is presented. It represents the most challenging problem of the three due to having many components (28 bodies in total), being made up of several different materials, and having many different heat generation sources.

Model Creation Process

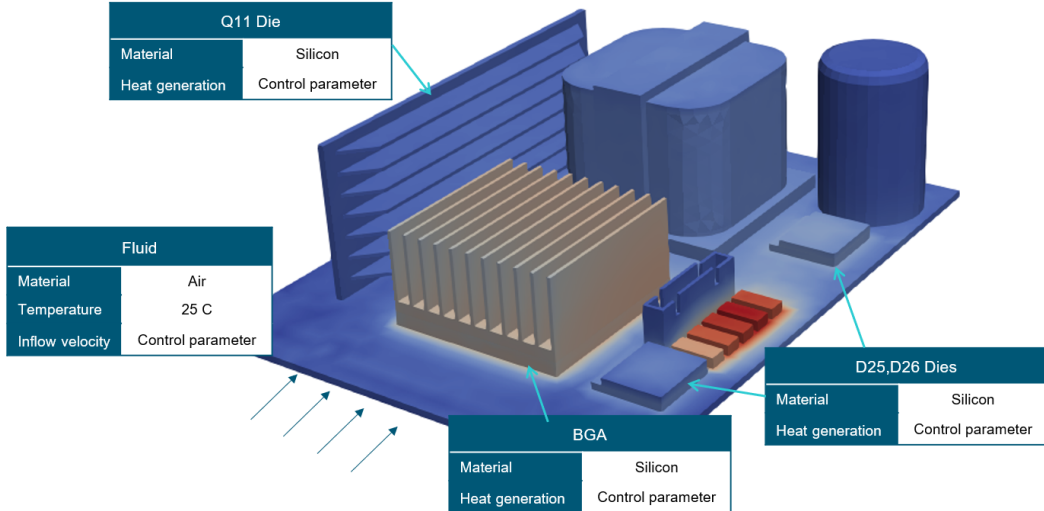


Figure 18: Basic problem geometry and flow depiction

The sampling of the DoE space is done via the same efficient space sampling method of the DoE space. The ranges of parameters for each axis are given in Table 5. 15 data points were used for the model creation process. The model training time was around 85 minutes (done on a Titan V GPU), and the total time taken to generate the model was around 200 minutes (which includes data generation time, created on an 8-core CPU machine).

Results

Figure 19 shows the temperature and pressure contours for a selected randomly drawn test point. Figures 19a and 19b show the temperature comparison, and Figures 19c and 19d show the pressure prediction. This qualitative accuracy of the test results versus CFD demonstrates the ability of the model to generalize well and predict flow-thermal results within the DoE design space, for very nontrivial geometries like the electronics box.

Parameter	Lower Value	Upper Value
Inflow Velocity (m/s)	0.5	5
Source Term(BGA) (W/m^3)	$1e^6$	$1e^7$
Source Term(D25 Die) (W/m^3)	$5e^6$	$5e^7$
Source Term(D26 Die) (W/m^3)	$5e^6$	$5e^7$
Source Term(Q11 Die) (W/m^3)	$1e^7$	$1e^8$

Table 5: DoE parameter ranges for the electronics box problem

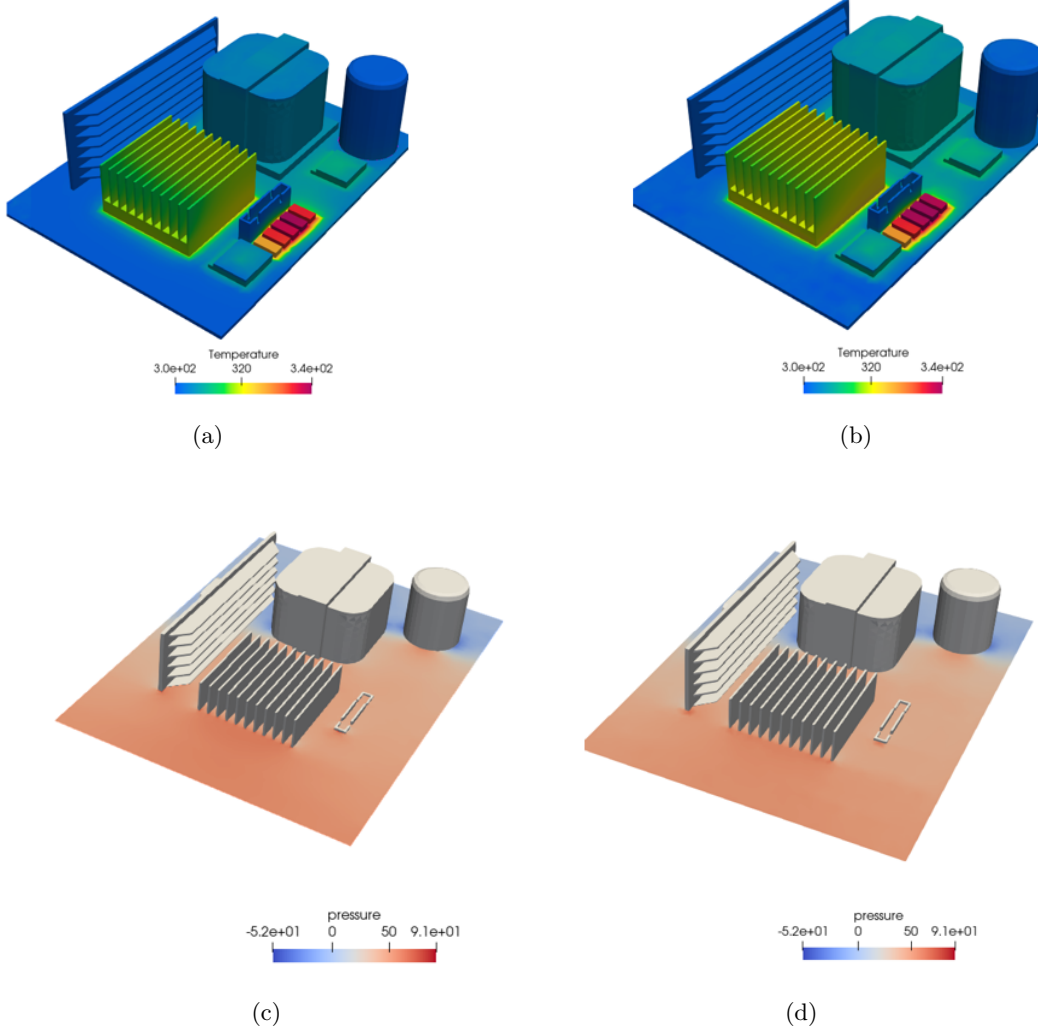


Figure 19: Comparisons between a commercial solver (Altair AcuSolve[®]) and the surrogate model.
(a) CFD temperature prediction on the test case (b) Model temperature prediction on the test case
(c) CFD pressure prediction on the test case (d) Model pressure prediction on the test case

5.2.4 Cost Benefit Analysis Compared to Standard CFD

In this section, a quantitative comparison of PINNs bases surrogate modeling versus CFD for DoE problems is presented. For the PINNs model training was performed on a single Titan V GPU card.

Heat Sink Design Optimization

Table 6 shows the cost-benefit analysis of the hybrid PINNs-CFD surrogate model versus CFD

for the heat sink design optimization problem shown in Section 5.2.1. The comparison, visualized in Figure 20 shows the total time taken to optimize the design using the PSO method and compares the time taken versus the number of iterations. The "model training time" encapsulates the time taken to create the data and train the model, so that it is a fair comparison.

Solve Type	Model Training Time	Time for a Design Iteration	Time for 10 Design Iterations
CFD (4 cores)	-	160 min	1600 min
PINN (1 GPU + 1 core)	286 mins	55 seconds	300 mins

Table 6: Comparing design iteration times using CFD versus ANN surrogate for the heatsink problem

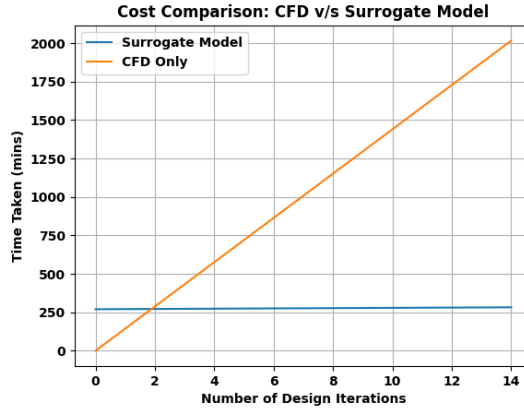


Figure 20: Time comparison of doing PSO-based design iterations using the surrogate versus CFD. Once the surrogate returns a truncated DoE space, the designer can perform high-fidelity CFD to fine-tune the design

PCB Thermal Analysis

Table 7 and Figure 21 shows a similar comparison for the PCB electronics assembly (see section 5.2.2). It is evident from both results that using accurate surrogate models can cap the cost of thoroughly solving DoE problems and reduce costs and increase efficiency.

Solve Type	Model Training Time	Time for each prediction
CFD (32 cores)	-	120 s
PINN (1 GPU + 1 core)	116 mins	3 seconds

Table 7: Comparing design iteration times using CFD versus ANN surrogate for the PCB design problem

5.2.5 Accuracy Comparisons

The created network models have several features that allow the creation of surrogates that are accurate, train quickly, and show good generalization capabilities. To demonstrate this, a few comparisons of predictions (for a test case) are shown, done with a standard fully connected network with none of the features that are described in Section 3, with predictions done using a model from the framework. These are example cases where using a standard data-driven network can lead to regions with unphysical results in the domain. Both models in both comparisons are created with the same dataset, the

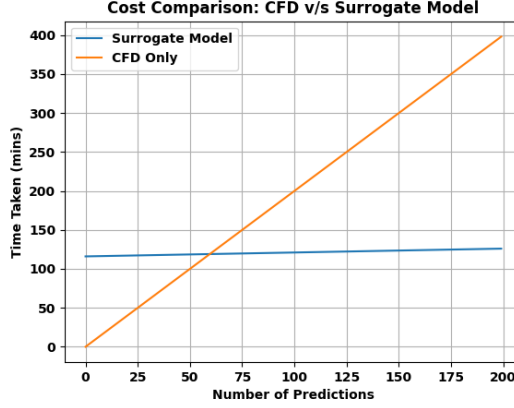


Figure 21: Comparison of time cost of using a surrogate to query versus CFD

same hyperparameters (besides those applicable to only Physics-ML models) and trained on the same hardware for the same number of iterations.

Example 1: Temperature on PCB

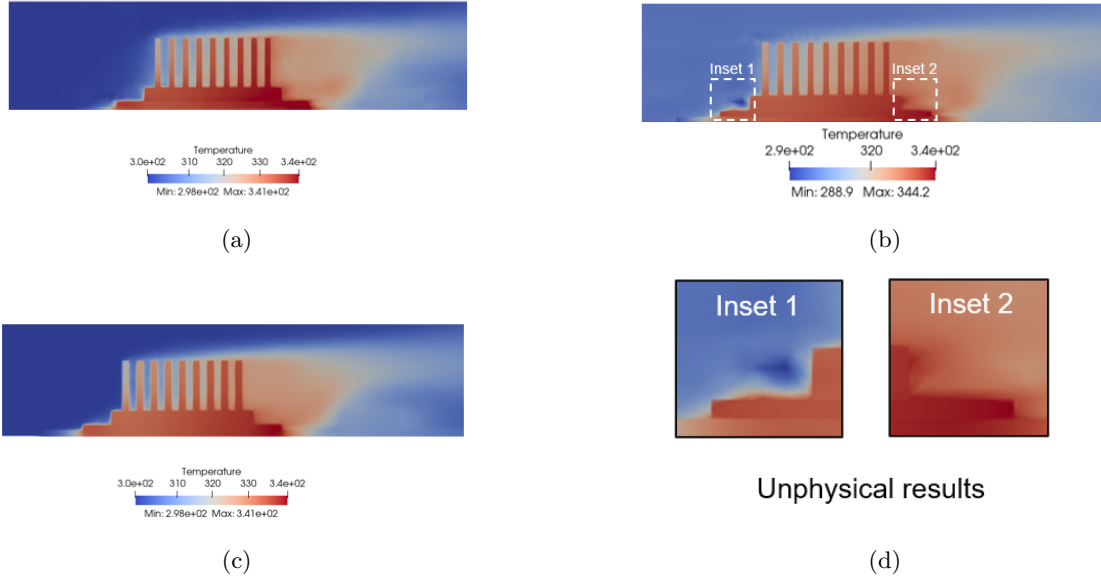


Figure 22: Temperature comparison on the PCB between predictions from standard data-driven NN versus PINN-based networks. (a) Prediction from framework network (b) Prediction from standard fully connected NN (c) True Solution (d) Insets from the prediction of standard NN showing unphysical results, especially near the boundaries

Figure 22 shows an example qualitative comparison of using models created by the framework versus standard data-driven models. The result from the standard data-driven model has regions of unphysical results, shown in Figure 22d.

Example 2: Pressure around Electronics Box

Figure 23 shows a similar difference in the accuracy of the result, in that the standard data-driven NN ends up with regions of non-physical results, all other applicable model creation parameters

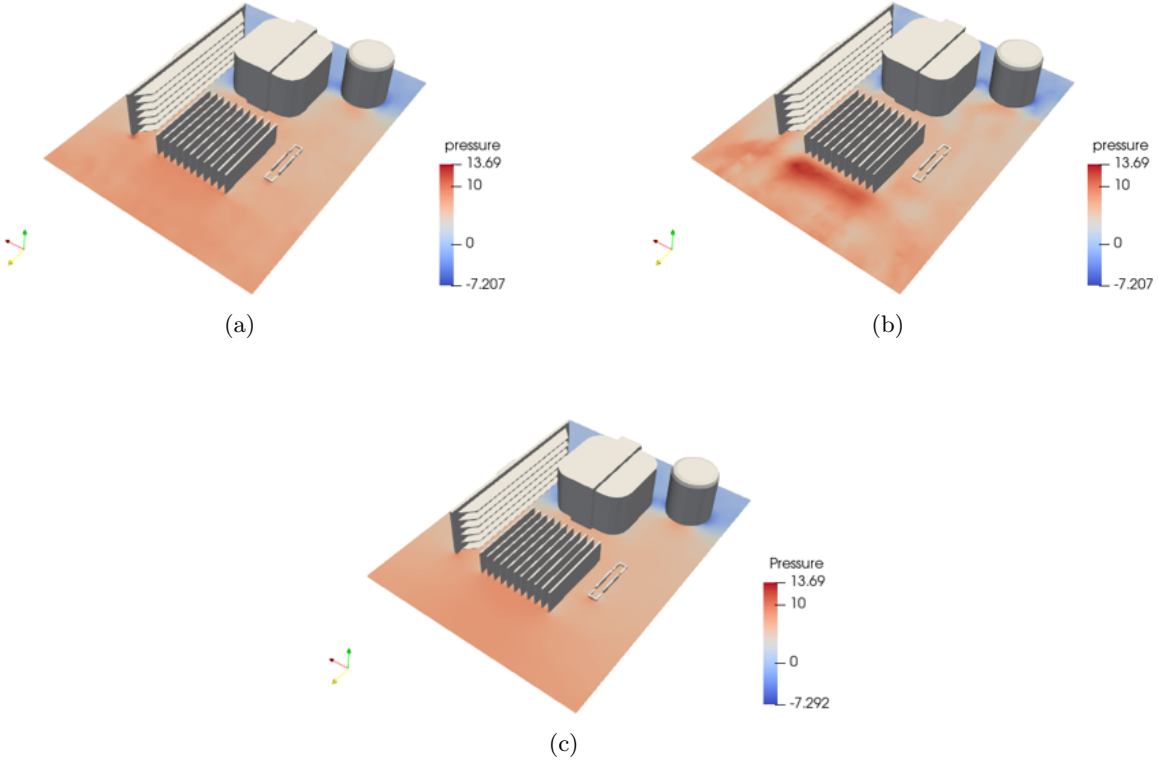


Figure 23: Pressure comparisons for flow over the electronics box (a) Prediction from framework network (b) Prediction from standard fully connected NN (c) True Solution

remaining the same.

5.2.6 Active Research Areas

Given that PINNs is such a promising yet young field, there are several areas of active research on applying them to different problems. A few pertinent ones are addressed here:

Turbulence Modeling

One unexplored area in PINNs is incorporating turbulence modeling into the learning process. Currently in the Altair framework, for creating surrogate models, the eddy viscosities from Altair AcuSolve® are used. Only very simple turbulence models have been implemented in 3D [25] for PINNs. Ghosh et al. [17] implemented the $\kappa - \epsilon$ 2 equation model for 2D flows, but this has yet to be extended to 3D. The lack of research on turbulence models for PINNs means that only the simplest turbulence models can be used currently, though Eivazi et al. [15] used PINNs to simulate simpler turbulent flow cases.

Geometry Parametrization

One of the most pressing problems that Neural Network based surrogate models have promised to solve is that of shape optimization. Design exploration by changing geometry is a time-consuming and complicated process in traditional CFD due to having to re-mesh for every small change, followed by running the solver. Yet, topology and shape optimization has become a key feature of most commercial solvers, highlighting the demand for the feature. The quick prediction capability of ANNs, coupled with the ability to predict on point clouds instead of meshes makes this method very promising in this application.

A recently popular approach is to use graph neural networks to read in point clouds or meshes directly [39, 45, 47], opening the door to exciting possibilities of parametrizing complex geometry relatively easily. There are also works using generative design and neural operators to solve problems of topology optimization. There have been several instances of solving these for structural problems but more recently there has been work solving flow-thermal topology optimization problems as well[43, 55, 61].

Uncertainty Quantification

One of the key metrics in being able to trust the results of ANN-based surrogates is to have a quantitative idea about the uncertainty of the prediction of the model. There has been a recent increase in the volume of works related to this topic [3, 71, 72], as practitioners and researchers have realized the importance of providing uncertainty measurements.

6 Conclusions and Future Work

In this paper, Physics Informed Neural Networks were introduced and some of their current limitations were discussed. Recent research on how to enhance the convergence properties of PINNs was discussed and a novel example in 3D was demonstrated, showing the benefit of adding physics to sparsely provided solution data. A demo problem solve was also demonstrated showing that PINNs can be used to solve realistic problems in a data-free manner for the 3D Navier Stokes equations. Their applications were also demonstrated for industry-grade flow-thermal surrogate modeling problems with the inclusion of some solution data and showed how combined with optimization algorithm models can arrive at optimal designs automatically based on user-defined constraints, in near real-time. It was also demonstrated that models from the framework perform better than basic data-driven ANNs for the exact same hyperparameters while showing the cost-benefit analysis for creating and using these models (including data creation and training time). The results shown in this paper can be built on to reduce surrogate cost creation, improve accuracy and reduce the black-box nature of ANN-based surrogate models.

There are multiple avenues through which the work shown in this paper can be improved. Research has to be done to improve convergence and offer guarantees of PINNs training toward the correct local minimums. This will further reduce data requirements for the creation of ANN-based surrogates. Further research also needs to be done for unsteady problems, which form an important class of problems that require surrogate models to model. More work needs to be done to incorporate and use other turbulence models with PINNs. Finally, one of the core issues with using physics-based regularizers is the additional cost they impose on the training process, and an important yet unexplored area of research is being able to use the physics regularization terms in a more memory and compute-efficient manner.

Acknowledgements

This research did not receive any specific grant from funding agencies in the public or not-for-profit sectors, or from any external commercial entities. The authors gratefully acknowledge the use of Altair Engineering Inc.’s computing facilities for running experiments.

CRedit authorship contribution statement

Saakaar Bhatnagar: Formal Analysis, Investigation, Methodology, Software, Validation, Writing-original draft. **Andrew Comerford:** Conceptualization, Investigation, Project Administration, Supervision, Writing- review and editing **Araz Banaeizadeh:** Conceptualization, Project Administration, Supervision, Writing- review and editing

References

- [1] Federico Antonello, Jacopo Buongiorno, and Enrico Zio. Physics informed neural networks for surrogate modeling of accidental scenarios in nuclear power plants. *Nuclear Engineering and Technology*, 2023.
- [2] Shamsulhaq Basir and Inanc Senocak. Critical investigation of failure modes in physics-informed neural networks. In *AIAA SCITECH 2022 Forum*. American Institute of Aeronautics and Astronautics, 2022. doi: 10.2514/6.2022-2353. URL <https://doi.org/10.2514%2F6.2022-2353>.
- [3] BVSS Bharadwaja, Mohammad Amin Nabian, Bharatkumar Sharma, Sanjay Choudhry, and Alankar Alankar. Physics-informed machine learning and uncertainty quantification for mechanics of heterogeneous materials. *Integrating Materials and Manufacturing Innovation*, 11(4):607–627, 2022.
- [4] Saakaar Bhatnagar, Yaser Afshar, Shaowu Pan, Karthik Duraisamy, and Shailendra Kaushik. Prediction of aerodynamic flow fields using convolutional neural networks. *Computational Mechanics*, 64:525–545, 2019.
- [5] Rafael Bischof and Michael Kraus. Multi-objective loss balancing for physics-informed deep learning. *arXiv preprint arXiv:2110.09813*, 2021.
- [6] Aniruddha Bora, Weizhong Dai, Joshua P Wilson, and Jacob C Boyt. Neural network method for solving parabolic two-temperature microscale heat conduction in double-layered thin films exposed to ultrashort-pulsed lasers. *International Journal of Heat and Mass Transfer*, 178:121616, 2021.
- [7] Steven L Brunton, Bernd R Noack, and Petros Koumoutsakos. Machine learning for fluid mechanics. *Annual review of fluid mechanics*, 52:477–508, 2020.
- [8] Shengze Cai, Zhiping Mao, Zhicheng Wang, Minglang Yin, and George Em Karniadakis. Physics-informed neural networks (pinns) for fluid mechanics: A review. *Acta Mechanica Sinica*, 37(12):1727–1738, 2021.
- [9] Shengze Cai, Zhicheng Wang, Sifan Wang, Paris Perdikaris, and George Em Karniadakis. Physics-Informed Neural Networks for Heat Transfer Problems. *Journal of Heat Transfer*, 143(6):060801, 2021. doi: 10.1115/1.4050542.
- [10] Giovanni Calzolari and Wei Liu. Deep learning to replace, improve, or aid cfd analysis in built environment applications: A review. *Building and Environment*, 206:108315, 2021.
- [11] Yuan Cao, Zhiying Fang, Yue Wu, Ding-Xuan Zhou, and Quanquan Gu. Towards understanding the spectral bias of deep learning. *arXiv preprint arXiv:1912.01198*, 2019.
- [12] Chen Cheng, Hao Meng, Yong-Zheng Li, and Guang-Tao Zhang. Deep learning based on pinn for solving 2 dof vortex induced vibration of cylinder. *Ocean Engineering*, 240:109932, 2021.
- [13] Ameya D. Jagtap and George Em Karniadakis. Extended physics-informed neural networks (xpinns): A generalized space-time domain decomposition based deep learning framework for nonlinear partial differential equations. *Communications in Computational Physics*, 10, 2020. doi: <https://doi.org/10.4208/cicp.OA-2020-0164>.
- [14] Jacob Devlin, Ming-Wei Chang, Kenton Lee, and Kristina Toutanova. Bert: Pre-training of deep bidirectional transformers for language understanding. *arXiv preprint arXiv:1810.04805*, 2018.
- [15] Hamidreza Eivazi, Mojtaba Tahani, Philipp Schlatter, and Ricardo Vinuesa. Physics-informed neural networks for solving reynolds-averaged navier–stokes equations. *Physics of Fluids*, 34(7), 2022. doi: 10.1063/5.0095270. URL <https://doi.org/10.1063%2F5.0095270>.
- [16] Chelsea Finn, Pieter Abbeel, and Sergey Levine. Model-agnostic meta-learning for fast adaptation of deep networks. In *International conference on machine learning*, pages 1126–1135. PMLR, 2017.
- [17] Shinjan Ghosh, Amit Chakraborty, Georgia Olympia Brikis, and Biswadip Dey. Rans-pinn based simulation surrogates for predicting turbulent flows. *arXiv preprint arXiv:2306.06034*, 2023.

[18] Rini J Gladstone, Mohammad A Nabian, and Hadi Meidani. Fo-pinns: A first-order formulation for physics informed neural networks. *arXiv preprint arXiv:2210.14320*, 2022.

[19] Xavier Glorot and Yoshua Bengio. Understanding the difficulty of training deep feedforward neural networks. In *Proceedings of the Thirteenth International Conference on Artificial Intelligence and Statistics*, Proceedings of Machine Learning Research, pages 249–256. PMLR, 2010.

[20] Gabriel FN Gonçalves, Assen Batchvarov, Yuyi Liu, Yuxin Liu, Lachlan R Mason, Indranil Pan, and Omar K Matar. Data-driven surrogate modeling and benchmarking for process equipment. *Data-Centric Engineering*, 1:e7, 2020.

[21] Vignesh Gopakumar, Stanislas Pamela, and Debasmita Samaddar. Loss landscape engineering via data regulation on pinns. *Machine Learning with Applications*, 12:100464, 2023.

[22] Xiaoxiao Guo, Wei Li, and Francesco Iorio. Convolutional neural networks for steady flow approximation. pages 481–490. Association for Computing Machinery, 2016. doi: 10.1145/2939672.2939738.

[23] Derek Hansen, Danielle Maddix Robinson, Shima Alizadeh, Gaurav Gupta, and Michael Mahoney. Learning physical models that can respect conservation laws. In *ICML 2023*, 2023.

[24] Haiyang He and Jay Pathak. An unsupervised learning approach to solving heat equations on chip based on auto-encoder and image gradient. *arXiv preprint arXiv:2007.09684*, 2020.

[25] Oliver Hennigh, Susheela Narasimhan, Mohammad Amin Nabian, Akshay Subramaniam, Kaus-tubb Tangsali, Zhiwei Fang, Max Rietmann, Wonmin Byeon, and Sanjay Choudhry. Nvidia simnet™: An ai-accelerated multi-physics simulation framework. In *International conference on computational science*, pages 447–461. Springer, 2021.

[26] Zheyuan Hu, Ameya D. Jagtap, George Em Karniadakis, and Kenji Kawaguchi. When do extended physics-informed neural networks (XPINNs) improve generalization? *SIAM Journal on Scientific Computing*, 44(5):A3158–A3182, 2022. doi: 10.1137/21m1447039. URL <https://doi.org/10.1137%2F21m1447039>.

[27] Kazuya Ishitsuka and Weiren Lin. Physics-informed neural network for inverse modeling of natural-state geothermal systems. *Applied Energy*, 337:120855, 2023. ISSN 0306-2619. doi: <https://doi.org/10.1016/j.apenergy.2023.120855>. URL <https://www.sciencedirect.com/science/article/pii/S0306261923002192>.

[28] Ameya D. Jagtap, Ehsan Kharazmi, and George Em Karniadakis. Conservative physics-informed neural networks on discrete domains for conservation laws: Applications to forward and inverse problems. *Computer Methods in Applied Mechanics and Engineering*, 365:113028, 2020. doi: <https://doi.org/10.1016/j.cma.2020.113028>.

[29] J. Kennedy and R. Eberhart. Particle swarm optimization. In *Proceedings of ICNN'95 - International Conference on Neural Networks*, volume 4, pages 1942–1948, 1995. doi: 10.1109/ICNN.1995.488968.

[30] Diederik P Kingma and Jimmy Ba. Adam: A method for stochastic optimization. *arXiv preprint arXiv:1412.6980*, 2014.

[31] Doyle Knight. *Design optimization in computational fluid dynamics*. Springer US, Boston, MA, 2001. doi: 10.1007/0-306-48332-7_90. URL https://doi.org/10.1007/0-306-48332-7_90.

[32] Elizabeth H. Krath, Forrest L. Carpenter, Paul G.A. Cizmas, and David A. Johnston. An efficient proper orthogonal decomposition based reduced-order model for compressible flows. *Journal of Computational Physics*, 426:109959, 2021. doi: 10.1016/j.jcp.2020.109959.

[33] Aditi Krishnapriyan, Amir Gholami, Shandian Zhe, Robert Kirby, and Michael W Mahoney. Characterizing possible failure modes in physics-informed neural networks. *Advances in Neural Information Processing Systems*, 34:26548–26560, 2021.

[34] Sangseung Lee and Donghyun You. Data-driven prediction of unsteady flow over a circular cylinder using deep learning. *Journal of Fluid Mechanics*, 879:217–254, 2019. doi: 10.1017/jfm.2019.700.

[35] Zongyi Li, Nikola B. Kovachki, Kamyar Azizzadenesheli, Burigede Liu, Kaushik Bhattacharya, Andrew M. Stuart, and Anima Anandkumar. Fourier neural operator for parametric partial differential equations. *CoRR*, 2020.

[36] Matti Lindstedt and Reijo Karvinen. Optimization of plate fin arrays with laminar and turbulent forced convection. In *Journal of Physics: Conference Series*, volume 395, page 012059. IOP Publishing, 2012.

[37] Ruo-Lin Liu, Yue Hua, Zhi-Fu Zhou, Yubai Li, Wei-Tao Wu, and Nadine Aubry. Prediction and optimization of airfoil aerodynamic performance using deep neural network coupled bayesian method. *Physics of Fluids*, 34(11), 2022.

[38] Zeyu Liu, Yantao Yang, and Qing-Dong Cai. Solving differential equation with constrained multilayer feedforward network. *arXiv preprint arXiv:1904.06619*, 2019.

[39] Andreas Mayr, Sebastian Lehner, Arno Mayrhofer, Christoph Kloss, Sepp Hochreiter, and Johannes Brandstetter. Boundary graph neural networks for 3d simulations. In *Proceedings of the AAAI Conference on Artificial Intelligence*, volume 37, pages 9099–9107, 2023.

[40] Luke Melas-Kyriazi. The mathematical foundations of manifold learning. *arXiv preprint arXiv:2011.01307*, 2020.

[41] Max D. Morris and Toby J. Mitchell. Exploratory designs for computational experiments. *Journal of Statistical Planning and Inference*, 43(3):381–402, 1995. ISSN 0378-3758. doi: [https://doi.org/10.1016/0378-3758\(94\)00035-T](https://doi.org/10.1016/0378-3758(94)00035-T).

[42] Akhil Nekkanti and Oliver T. Schmidt. Gappy spectral proper orthogonal decomposition. *Journal of Computational Physics*, 478:111950, 2023. doi: 10.1016/j.jcp.2023.111950.

[43] Sangeun Oh, Yongsu Jung, Seongsin Kim, Ikkjin Lee, and Namwoo Kang. Deep Generative Design: Integration of Topology Optimization and Generative Models. *Journal of Mechanical Design*, 141(11):111405, 2019. doi: 10.1115/1.4044229.

[44] Jan Oldenburg, Finja Borowski, Alper Öner, Klaus-Peter Schmitz, and Michael Stiehm. Geometry aware physics informed neural network surrogate for solving navier–stokes equation (gapinn). *Advanced Modeling and Simulation in Engineering Sciences*, 9(1):8, 2022. doi: <https://doi.org/10.1186/s40323-022-00221-z>.

[45] Luca Pegolotti, Martin R Pfaller, Natalia L Rubio, Ke Ding, Rita Brugarolas Brufau, Eric Darve, and Alison L Marsden. Learning reduced-order models for cardiovascular simulations with graph neural networks. *arXiv preprint arXiv:2303.07310*, 2023.

[46] Michael Penwarden, Shandian Zhe, Akil Narayan, and Robert M Kirby. A metalearning approach for physics-informed neural networks (pinns): Application to parameterized pdes. *Journal of Computational Physics*, 477:111912, 2023.

[47] Tobias Pfaff, Meire Fortunato, Alvaro Sanchez-Gonzalez, and Peter W Battaglia. Learning mesh-based simulation with graph networks. *arXiv preprint arXiv:2010.03409*, 2020.

[48] Nasim Rahaman, Aristide Baratin, Devansh Arpit, Felix Draxler, Min Lin, Fred Hamprecht, Yoshua Bengio, and Aaron Courville. On the spectral bias of neural networks. In *International Conference on Machine Learning*, pages 5301–5310. PMLR, 2019.

[49] M. Raissi, P. Perdikaris, and G.E. Karniadakis. Physics-informed neural networks: A deep learning framework for solving forward and inverse problems involving nonlinear partial differential equations. *Journal of Computational Physics*, 378:686–707, 2019. doi: <https://doi.org/10.1016/j.jcp.2018.10.045>.

[50] Maziar Raissi and George Em Karniadakis. Hidden physics models: Machine learning of nonlinear partial differential equations. *Journal of Computational Physics*, 357:125–141, 2018. doi: 10.1016/j.jcp.2017.11.039.

[51] Aditya Ramesh, Mikhail Pavlov, Gabriel Goh, Scott Gray, Chelsea Voss, Alec Radford, Mark Chen, and Ilya Sutskever. Zero-shot text-to-image generation. In *International Conference on Machine Learning*, pages 8821–8831. PMLR, 2021.

[52] Chengping Rao, Hao Sun, and Yang Liu. Physics-informed deep learning for computational elastodynamics without labeled data. *Journal of Engineering Mechanics*, 147(8):04021043, 2021.

[53] Nadim Saad, Gaurav Gupta, Shima Alizadeh, and Danielle Maddix Robinson. Guiding continuous operator learning through physics-based boundary constraints. In *ICLR 2023*, 2023.

[54] Rahul Sharma, Maziar Raissi, and Yuebin Guo. Physics-informed deep learning of gas flow-melt pool multi-physical dynamics during powder bed fusion. *CIRP Annals*, 2023. doi: <https://doi.org/10.1016/j.cirp.2023.04.005>.

[55] Khemraj Shukla, Vivek Oommen, Ahmad Peyvan, Michael Penwarden, Luis Bravo, Anindya Ghoshal, Robert M Kirby, and George Em Karniadakis. Deep neural operators can serve as accurate surrogates for shape optimization: a case study for airfoils. *arXiv preprint arXiv:2302.00807*, 2023.

[56] Vincent Sitzmann, Julien Martel, Alexander Bergman, David Lindell, and Gordon Wetzstein. Implicit neural representations with periodic activation functions. *Advances in neural information processing systems*, 33:7462–7473, 2020.

[57] Hwijae Son, Sung Woong Cho, and Hyung Ju Hwang. Enhanced physics-informed neural networks with augmented lagrangian relaxation method (al-pinn). *Neurocomputing*, page 126424, 2023.

[58] Shashank Subramanian, Robert M Kirby, Michael W Mahoney, and Amir Gholami. Adaptive self-supervision algorithms for physics-informed neural networks. *arXiv preprint arXiv:2207.04084*, 2022.

[59] N. Sukumar and Ankit Srivastava. Exact imposition of boundary conditions with distance functions in physics-informed deep neural networks. *Computer Methods in Applied Mechanics and Engineering*, 389:114333, 2022. doi: 10.1016/j.cma.2021.114333.

[60] Luning Sun, Han Gao, Shaowu Pan, and Jian-Xun Wang. Surrogate modeling for fluid flows based on physics-constrained deep learning without simulation data. *Computer Methods in Applied Mechanics and Engineering*, 361:112732, 2020. doi: 10.1016/j.cma.2019.112732.

[61] Yubiao Sun, Ushnish Sengupta, and Matthew Juniper. Physics-informed deep learning for simultaneous surrogate modeling and pde-constrained optimization of an airfoil geometry. *Computer Methods in Applied Mechanics and Engineering*, 411:116042, 2023. doi: <https://doi.org/10.1016/j.cma.2023.116042>.

[62] Matthew Tancik, Pratul Srinivasan, Ben Mildenhall, Sara Fridovich-Keil, Nithin Raghavan, Utkarsh Singhal, Ravi Ramamoorthi, Jonathan Barron, and Ren Ng. Fourier features let networks learn high frequency functions in low dimensional domains. *Advances in Neural Information Processing Systems*, 33:7537–7547, 2020.

[63] Gaël Varoquaux and Veronika Cheplygina. Machine learning for medical imaging: methodological failures and recommendations for the future. *NPJ digital medicine*, 5(1):48, 2022.

[64] Sifan Wang, Yujun Teng, and Paris Perdikaris. Understanding and mitigating gradient flow pathologies in physics-informed neural networks. *SIAM Journal on Scientific Computing*, 43(5): A3055–A3081, 2021. doi: 10.1137/20M1318043.

[65] Sifan Wang, Hanwen Wang, and Paris Perdikaris. Learning the solution operator of parametric partial differential equations with physics-informed deepnets. *Science Advances*, 7(40):eabi8605, 2021. doi: 10.1126/sciadv.abi8605.

- [66] Sifan Wang, Shyam Sankaran, and Paris Perdikaris. Respecting causality is all you need for training physics-informed neural networks. *arXiv preprint arXiv:2203.07404*, 2022.
- [67] Sifan Wang, Hanwen Wang, and Paris Perdikaris. Improved architectures and training algorithms for deep operator networks. *Journal of Scientific Computing*, 2022.
- [68] Sifan Wang, Xinling Yu, and Paris Perdikaris. When and why pinns fail to train: A neural tangent kernel perspective. *Journal of Computational Physics*, 449:110768, 2022.
- [69] Benjamin Wu, Oliver Hennigh, Jan Kautz, Sanjay Choudhry, and Wonmin Byeon. Physics informed rnn-dct networks for time-dependent partial differential equations. In *International Conference on Computational Science*, pages 372–379. Springer, 2022.
- [70] Kailai Xu and Eric Darve. Physics constrained learning for data-driven inverse modeling from sparse observations. *Journal of Computational Physics*, 453:110938, 2022. ISSN 0021-9991. doi: <https://doi.org/10.1016/j.jcp.2021.110938>. URL <https://www.sciencedirect.com/science/article/pii/S0021999121008330>.
- [71] Liu Yang, Xuhui Meng, and George Em Karniadakis. B-pinns: Bayesian physics-informed neural networks for forward and inverse pde problems with noisy data. *Journal of Computational Physics*, 425:109913, 2021.
- [72] Dongkun Zhang, Lu Lu, Ling Guo, and George Em Karniadakis. Quantifying total uncertainty in physics-informed neural networks for solving forward and inverse stochastic problems. *Journal of Computational Physics*, 397:108850, 2019. doi: 10.1016/j.jcp.2019.07.048. URL <https://doi.org/10.1016%2Fj.jcp.2019.07.048>.
- [73] Yaomin Zhao, Harshal D Akolekar, Jack Weatheritt, Vittorio Michelassi, and Richard D Sandberg. Rans turbulence model development using cfd-driven machine learning. *Journal of Computational Physics*, 411:109413, 2020.